Journal of the Korean Magnetic Resonance Society **2004**, *8*, 1 - 18

Decreased entropy of unfolding increases the temperature of maximum stability : Thermodynamic stability of a thioredoxin from the hyperthermophilic archaeon *Methanococcus jannaschii*

Duck Yeon Lee, Kyeong-Ae Kim, and Key-Sun Kim*

Structural Biology Center, Korea Institute of Science and Technology,
Cheongyang Box 131, Seoul, 130-650, Korea
Received February 8, 2004

Abstract : A thioredoxin from hyperthermophile, *Methanococcus jannashii* (*Mj*TRX) was characterized by use of the differential scanning calorimetry to understand the mechanisms of thermodynamic stability. *Mj*TRX has an unfolding transition temperature of 116.5 °C, although the maximum free energy of the unfolding (9.9 Kcal/mol) is similar to that of *E. coli* thioredoxin (*E*TRX, 9.0 Kcal/mol). However, the temperature of maximum stability is higher than *E*TRX by 20 °C, indicating that the unfolding transition temperature increased by shifting the temperature of maximum stability. *Mj*TRX has lower enthalpy and entropy of the unfolding compared to *E*TRX maintaining a similar free energy of the unfolding. From the structure and the thermodynamic parameters of *Mj*TRX, we showed that the unfolding transition temperature of *Mj*TRX is increased due to the decreased entropy of the unfolding. Decreasing the unfolded state entropy and increasing the folded state entropy can decrease the entropy of the unfolding. In the case of *Mj*TRX, the increased number of proline residues decreased the unfolded state entropy and the increased enthalpy in the folded state increased the folded state entropy.
Keyword: maximum stability temperature, entropy, structure, *Mj*TRX

INTRODUCTION

Increased enthalpy or decreased entropy of the unfolding can stabilize protein in theory. So, decreasing enthalpy or increasing entropy in the folded state would stabilize proteins. The decreased enthalpy in the folded state is achieved by many favorable interactions, and increased entropy in the folded state represents the increased flexibility of

* To whom correspondence should be addressed. E-mail: keysun@kist.re.kr

protein. Strong interactions between two chemical groups generally decrease the flexibility of protein, resulting in the increased rigidity of protein. It is believed that a rigid protein is more stable than a flexible protein in that regard. But increased flexibility could increase the stability if the enthalpy-entropy compensation is favorable for the protein stability. One the other hand, the decreased entropy in the unfolded state could decrease entropy of the unfolding, resulting in increased stability of proteins. Introduction of disulfide bonds or proline residues was shown to be effective in decreasing entropy in the unfolded state.[1]

Thus far, many thermophilic proteins have been shown to contain an increased number of salt bridges that are often involved in networks at inter-domain and at inter-subunit interfaces [2-7] ; extra proline residues[8]; more aromatic-aromatic interactions [9]; more hydrophobic interactions [10] ; and high order of oligomerization (reviewed in ref.11). These interactions increase the unfolding transition temperature. However, it is not clear yet how these interactions affect the thermodynamic parameters that result in the high unfolding transition temperature.

In this report, we characterized a thioredoxin from the hyperthermophilic archaeon *Methanococcus jannaschii* (*Mj*TRX) and showed that *Mj*TRX has a high unfolding transition temperature owing to the decreased entropy of the unfolding. The decreased entropy of the unfolding shifted the temperature of maximum stability to the higher temperature, resulting in the high unfolding transition temperature.

MATERIALS AND METHODS

Protein expression and Purification

The *Mj*TRX gene was sub-cloned into the expression vector pET15b (Novagen) (Lee et al., 2000). *E. coli* BL21 (DE3) harboring each recombinant plasmid was grown at 37 °C until $A_{600} \cong 1$, and the recombinant proteins were induced with 0.4 mM isopropyl-1-thio-β-D-galatopyranoside for 2 hrs. Cell paste obtained by centrifugation at 5,000 rpm for 15 min. was re-suspended in a lysis buffer (50 mM potassium phosphate, pH 8.0, and 300 mM KCl) and disrupted by ultrasonication. DNase I (10μg/ml) and RNase (10μg/ml) were added to the cell extract and incubated for 30 min. at room temperature to remove nucleic acid. The crude extract was heated at 85 °C for 30 min, and centrifuged at 16,000 rpm for 20 min.

The supernatant was loaded onto a Nickel nitrilotriacetic acid-agarose resin (Ni-NTA) column (Qiagen) and eluted with an elution buffer (50 mM potassium phosphate, pH 6.0, 300 mM KCl, and 10 % glycerol) containing 0.3 M imidazole. The polyhistidine tag was removed by thrombin for 12 hrs at room temperature. The cleaved protein solution was dialyzed and loaded onto a DEAE-Sepharose column equilibrated with dialysis buffer (50 mM potassium phosphate, pH 6.5, and 2 mM EDTA). The flow-through was concentrated by ultrafiltration using an Amicon ultrafiltration apparatus (Amicon). The concentrated sample was further purified by gel filtration chromatography using a Superdex G75 column (Pharmacia, 1 cm x 30 cm) in 50 mM potassium phosphate (pH 6.5), 2 mM EDTA, and 300 mM KCl. Purified protein was verified by the N-terminal amino acid sequencing at Korea Basic Science Institute (KBSI) in Seoul. *Mj*TRX has the N-terminal extension of Gly-Ser-His. *E*TRX was expressed and purified as described by Langsetmo *et al.* [12] with anion exchange and gel filtration chromatography. The uniform isotope labeling of ^{13}C, ^{15}N atoms in *Mj*TRX was achieved by growing cells in M9 minimal medium with 1.0 g of $^{15}NH_4Cl$/liter and 2.0 g of ^{15}C-glucose/liter. NMR samples were prepared by dissolving about 10 mg of protein in 0.5 ml of either 90% H_2O/10% ^2H_2O or 99.9% ^2H_2O. The pH was adjusted to 3.30±0.05 (glass electrode, uncorrected) with concentrated NaO^2H.

Differential Scanning Calorimetry

Differential scanning calorimetry (DSC) was carried out with a nano-Differential Scanning Calorimetry (Calorimetry Sciences Corp. U.S.A.) at a heating rate of 1℃/min. Sample proteins of 0.3 to 1.5 mg/ml were used for analysis after dialyzing against the reference buffer overnight. Reference buffers were 50mM potassium phosphate with varying pH from 3 to 9 and guanidine thiocyanate (GdnSCN) up to 1.4M was added to the sample at pH 6.5 to shift the unfolding transition temperature. The concentration of *Mj*TRX and *E*TRX was determined using molar extinction coefficients of 3,105 and 13,700 $M^{-1}cm^{-1}$ at 280 nm, respectively. A partial specific volume of 0.74 ml/g and a molecular weight of 9,687 for *Mj*TRX estimated by a program SEQSEE [13] was used for the analysis of DSC data The maximum stability of *E*TRX was calculated from the previously reported thermodynamic parameters of *E*TRX (106.9 ±1.1 Kcal mol^{-1}, 297±3 cal mol^{-1} $°K^{-1}$ and 1.66 ± 0.05 kcal $mol^{-1}deg^{-1}$ for enthalpy, entropy and heat capacity, respectively at the unfolding

transition temperature of 87 °C in 10 mM phosphate buffer, pH 7.0 with 0.1 N NaCl .[1]

Cicular Dichroism Spectra

Far-UV circular dichroism (CD) spectra were recorded on a Jasco715 spectropolarimeter equipped with an IBM personal computer at a scan rate of 20 nm/min, using a time constant of 0.25 sec. The path length of the cell was 0.1 cm and each scan was recorded from 270 to 190 nm. Denaturant-induced unfolding of *Mj*TRX was performed at several temperatures in the presence of GdnSCN at pH 6.5 in 10mM potassium phosphate The concentration of *Mj*TRX was 0.1~0.35mg/ml.

NMR Spectroscopy

The heteronuclear NMR experiments were carried out with ^{15}N labeled *Mj*TRX wild type and E25/36/51D triple mutant sample in 90%H_2O/10%^2H_2O. All experiments were done using Varian UNITY *plus* 600 Spectrometer (at Advance Analysis Center of KIST) at 30 °C. The concentration of protein was about 2 mM. Two-dimensional ^1H-^{13}C constant time HSQC, 3D ^1H -^{15}N NOESY-HSQC, ^1H -^{15}N TOCSY-HSQC, [15] HNHA, [16] HCACO [17] and HNCO[18] were acquired with the ^{13}C- or ^{15}N-labeled sample, and ^{13}C-, ^{15}N-edited NOESY,[19] HNCACB and CBCA(CO)NH [20] were acquired with the ^{13}C-, ^{15}N-labeled sample NMR data were processed using the program NMRPipe.[21]

Assignments and Distance Restraints

Starting with the identifications of ^{15}N- and HN-chemical shifts in ^1H-^{15}N HSQC, spin systems were partially identified in ^1H-^{15}N TOCSY-HSQC, and the sequential assignments of each amino acid were made using HNCACB, CBCA(CO)NH, and ^1H-^{15}N NOESY-HSQC with a mixing time of 120 ms. Chemical shift indices were calculated by the method of Wishart et al. [22] NOE distance restraints were derived from 3D ^{13}C-, ^{15}N-edited NOESY with a mixing time of 120 ms. All NOE cross peaks were assigned using a program PIPP. The NOE intensity was converted into three groups of classes (1.8-2.7, 1.8-3.5, and 1.8-5.0). The $^3J_{HNH\alpha}$ scalar-coupling constant of the α-proton to the amide proton was obtained from the HNHA experiments. The backbone torsion angle ϕ was restrained to -85 to -25 for $^3J_{HNH\alpha}$ < 5.5Hz, -70 to -170 for $^3J_{HNH\alpha}$ 8-9 Hz. The ψ torsion angles were

restrained to -70 to –10 for the helix and to 85 to 175. The side chain torsion angles χ_1 were restrained based on cross peak intensities deduced from ^{15}N-edited TOCSY and ^{15}N-edited NOESY spectra.[23] Additional backbone H-bond restraints were given where secondary structures were indicated, based on NOE connectivity. For each hydrogen bond, two restraints (r_{NH-O}, 1.7-2.3; r_{N-O}, 2.5-3.3) were used. Additionally, $^3J_{HNH\alpha}$-coupling constants [24] were directly included in the simulated annealing protocol during refinement.

Structure Calculation

The structures were calculated with a distance geometry and simulated annealing protocol using an X-PLOR program. [25] The secondary structures were initially identified with the chemical shift index,[26] $^3J_{HNH\alpha}$-coupling constants, and medium range NOE connectivity.[27] In the initial structure calculations from an extended chain, NOE restraints and hydrogen bonds in the helix region were included. When the initial structures were obtained, $^3J_{HNH\alpha}$-coupling constants and dihedral angles were included. During the calculations, ambiguous assignments were clarified and the refinements of structures were achieved with the inclusion of the chemical shift database potential. [28-29]

RESULTS

Differential Scanning Calorimetry of MjTRX

The thermodynamic stability of *Mj*TRX was examined by differential scanning calorimetry (DSC) and compared to well-characterized *E. coli* thioredoxin, *E*TRX. As observed in other hyperthermophilic proteins,[30] the heat denaturation of *Mj*TRX was not reversible under the conditions used in DSC experiments. However, heat-denaturation of *Mj*TRX was not accompanied by further heat absorbing or releasing processes, and the heat-denatured samples were clear after cooling down to the room temperature, indicating that the unfolded chains did not aggregate (Fig. 1). Therefore, the unfolding process could be interpreted thermodynamically.[31-32] When denaturants such as GdnSCN were added to the samples, the temperatures of the unfolding transition (T_m) and the enthalpy of the unfolding (ΔH_m) were linearly dependent on the concentration of denaturant (Fig. 1). The thermodynamic parameters were also obtainable between pH 3.0-3.5 without adding

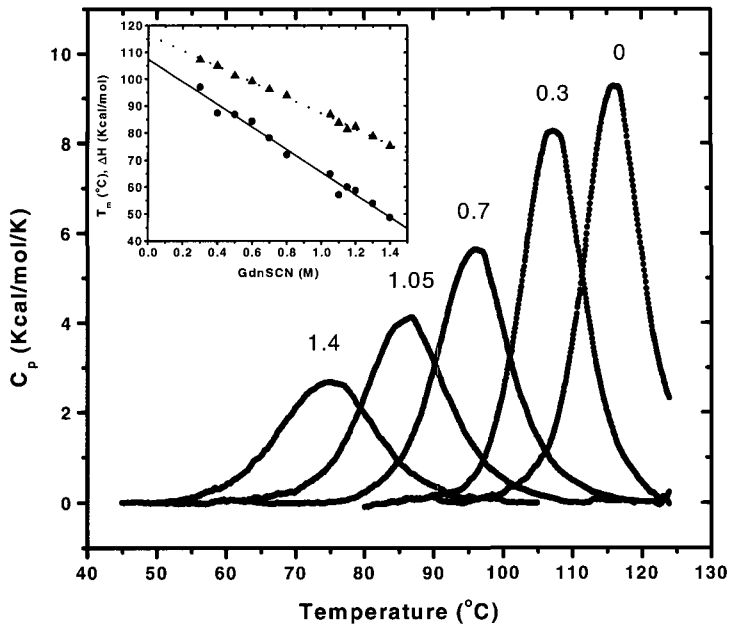

Fig. 1. Thermograms of *Mj*TRX at various GdnSCN concentrations. The concentration of GdnSCN is written on the thermograms. The graphs in the inset indicate the unfolding transition temperatures and the enthalpies of the unfolding dependent on the concentration of GdnSCN.

denaturants with the unfolding transition temperature of 92-96 °C. It was not possible to get thermodynamic parameters at other higher or lower pHs because the proteins aggregated at high temperature or unfolded at too high temperatures. Extrapolation of the measured T_m and ΔH_m to zero denaturant concentration yields T_m of 116.5±0.6°C and ΔH_m of 107.3 ± 1.7 kcal mol^{-1}, respectively. Extrapolated T_m is the same value observed at pH 6.5 in 50 mM potassium phosphate buffer. All thermograms at the measured denaturant concentrations show two-state transition behavior and were independent of scan rates (data not shown), indicating that the native and unfolded forms equilibrate rapidly in comparison with the time constant of the instrument. Also the concentration of *Mj*TRX (from 0.3 to 3 mg/ml) did not affect T_m of proteins indicating the absence of oligomerization.[33] Enthalpies of the unfolding at transition temperatures (ΔH_{cal}) were a linear function of T_m (Fig. 2) in the range of temperatures 75-110 °C with the apparent ΔC_p of 1.41 ± 0.06 kcal $mol^{-1}deg^{-1}$.

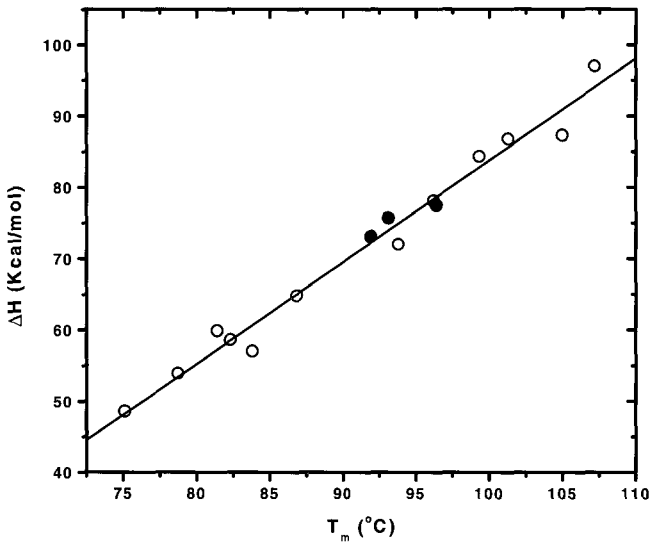

Fig. 2. The correlation of the enthalpy of unfolding and the unfolding transition temperature. Open circles are from the thermal unfolding at pH 6.5 with GdnSCN and closed circles are from the thermal unfolding at pH 3.0, 3.2 and 3.6. The ΔC_P of 1.4 kcal/mol/K are obtained from the slope.

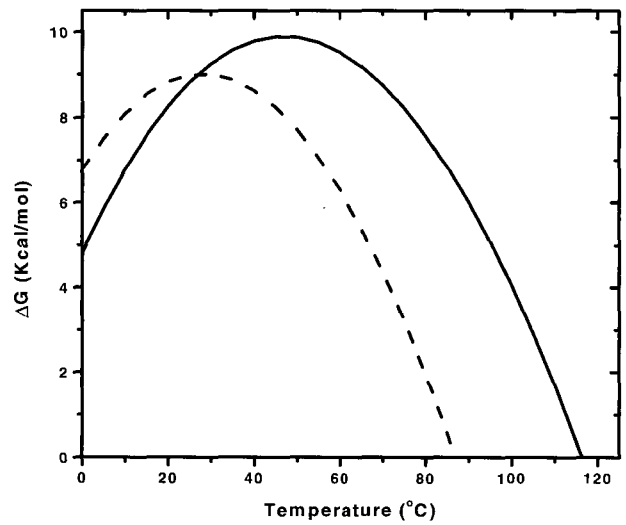

Fig. 3. Temperature dependency of free energies of *Mj*TRX (solid line) and *E*TRX (dotted line). The maximum free energies of *Mj*TRX and *E*TRX are 9.9 Kcal/mol at 47°C and 9.0 Kcal/mol at 28°C.

Enthalpy and entropy (ΔS_m) of the unfolding at the transition temperature were 107.3 ± 1.7 kcal mol^{-1} and 275 ± 5 cal $mol^{-1}deg^{-1}$, respectively. These parameters were used in conjunction with the Gibbs-Helmholtz equation (Eq. 1) to evaluate $\Delta G°$ at the given temperature.

$$\Delta G\,(T) = \Delta H_o\,(1\text{-}T\,/T_o) + \Delta C_p\,[(T - T_o) - T\ln(T\,/T_o)] \qquad \text{(Eq. 1)}$$

The temperature dependency of the free energy of the unfolding of *Mj*TRX shows that the temperature of maximum stability is shifted to the higher temperature around 47 °C, compared to the mesophilic proteins that have the maximum stability around 10 °C .[34] However, the maximum free energy of the unfolding of *Mj*TRX (9.9 Kcal mol^{-1}) is close to that of *E*TRX (9.0 Kcal mol^{-1}). The maximum free energy of the unfolding of *E*TRX was obtained around 28 °C (Fig. 3). On the other hand, the heat capacity of *Mj*TRX (1.41 ± 0.06 kcal $mol^{-1}deg^{-1}$) was smaller than that of *E*TRX (1.66 ± 0.05 kcal $mol^{-1}deg^{-1}$).

Solution structure of MjTRX

The structure of *Mj*TRX was determined to see whether there are any structural reasons for the higher unfolding transition temperature. The three dimensional structure of *Mj*TRX was defined by 1128 experimentally derived NOE distance restraints, 120 dihedral angle restraints, 36 hydrogen bonds, and 67 $^3J_{HNH\alpha}$ coupling constants. The root mean square deviation for backbone and all heavy atoms of 20 minimized structures around mean atomic displacements of the whole molecule (residues Met^1-Leu^{85}) was 0.63 and 1.06 Å and those of well structured regions (residues 4 to 85) are 0.48 and 0.92 Å, respectively. More than 85% of residues is in the most favorable region in Ramachandran plot (Table 1) with no violation of NOE restraints greater than 0.5 Å and dihedral angles greater than 5°. The three-dimensional structure consists of three α-helices (residues 16-30, 46-52 and 74-84) and 4 β-sheet (residues 4-10, 35-41, 60-62 and 65-68) arranged in βαβαββα similar to a glutaredoxin. Among the β-sheet, β3 and β4 (60-62 and 65-68) are short and not very well defined, which is found in 15 low energy structures out of 20 (Fig. 4). The electrostatic potential surface of *Mj*TRX indicates that the hydrophobic surface is exposed around the active site but the other side of protein is negatively charged. The secondary structures of

these regions are somewhat deviated from the regions predicted by the chemical shift index[35]. The structure of *Mj*TRX at 30 C, pH3.3 obtained in this study is consistent with the structure at 60 C, pH 6.1. [36]

Table 1. Summary of structural restraints derived from NOEs, coupling constants.

NOE distance restraints			
Intra-residual	533		
Sequential	250		
Medium-range($1<\|i-j\|\leq 4$)	155		
Long-range($\|i-j\|\geq 5$)	190		
Hydrogen bonds	2*36[a]		
Angular restraints:			
Dihedral angle ψ	47		
Dihedral angle χ^1	28		
Coupling constants	67		
Ramachandran plot[b]			
Most favorable region	87.2		
Additionally allowed region	12.2		
Generously allowed region	0.6		
Dihedral angle ϕ	45		
Disallowed region	0.0		
Atomic rmsd values(Å)	residues 4-85		
Backbone atoms	0.48		
Heavy atoms	0.92		
X-PLOR energy terms (kcal/mol)			
E_{tot}	-281	±	40.9
E_{bond}	23	±	2.8
E_{angle}	202	±	6.0
$E_{improper}$	32	±	3.1
E_{vdw}	-640	±	32
E_{cdih}	1	±	0.4
E_{NOE}	101	±	14.3

[a] For each hydrogen bond, two distance restraints are used : r_{HN-O} 1.7-2.3, r_{N-O} 2.5-3.3. Coupling constants are used for restraints based on Clore and co-workers.[28] Coupling constants are values obtained from HNHA experiments. [b] The program PROCHECK_nmr [43] was used to analyze the quality of the structure. The values for X-PLOR energy terms were obtained with force constraints of 4 kcal/mol/Å^4 (E_{vdw}), 50 kcal/mol/Å^2 (E_{NOE}), and 200 kcal/mol (E_{cdih}). E_{vdw} energy is L-J energy of XPLOR [25] energy terms.

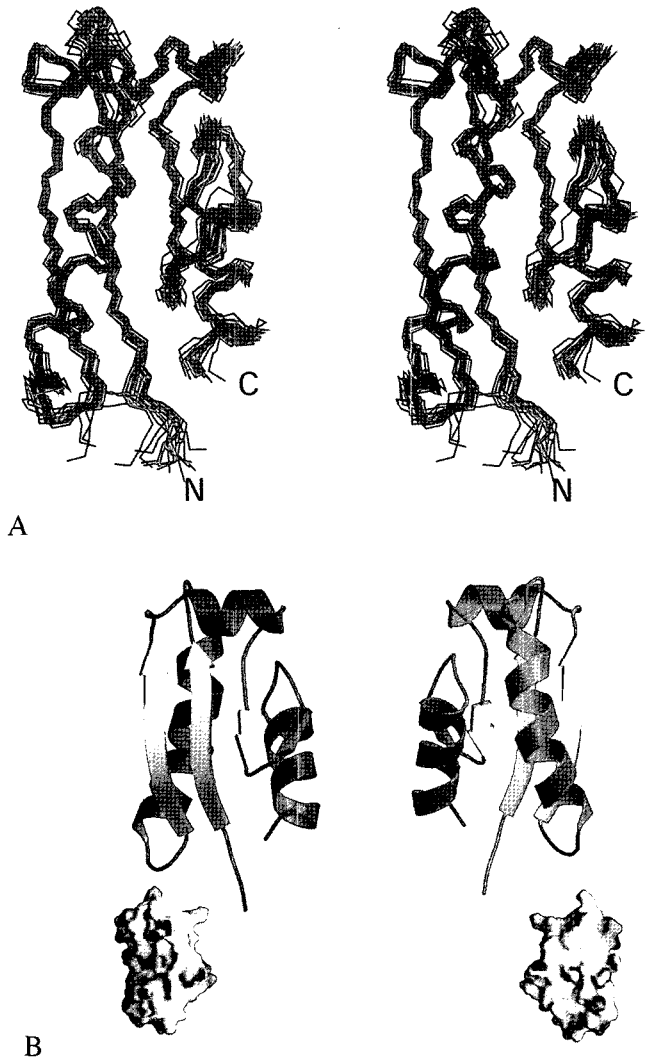

Fig. 4. Structure of *Mj*TRX. A, stereoview of the backbone atoms (N, Ca, C') of 20 structures of *Mj*TRX. The root mean square deviation about the mean coordinate position for residues 4-85 is 0.48 Å for the backbone atoms and 0.92 Å for all heavy atoms. Other structural statistics are summarized in Table 1. B, ribbon drawing of the *Mj*TRX. The view is the same as in A in the left and opposite side of view in the right. The active site disulfide bridge is shown in the right. At the bottom of each ribbon drawing, the electrostatic potential surface of *Mj*TRX is shown in the same view as in ribbon drawing. The electrostatic potential surface is color-coded with the negatively charged surface in red (<– 15 K_BT) and the positively charged surface in blue (>15 K_BT). Ribbon drawing was generated by programs MOLSCRIPT [44] and RASTER3D,[45] and electrostatic potential surface was generated by a program GRASP .[46]

DISCUSSION

The increased thermodynamic stability seems to be acquired by a protein through the small structural modifications that affect the thermodynamic parameters such as enthalpy and entropy of the unfolding. Many researchers have reported that the hyperthermophilic protein is stabilized by ion-pairs–the so called 'ion-network'– [2, 37] and so is highly dependent on the salt concentration. The unfolding transition temperature of a methionine aminopeptidase from *Pyrococcus furiosus* is decreased by 25°C in a buffer containing 100mM of KCl.[38] In the case of *Mj*TRX, the unfolding transition temperatures were changed less than 4 °C with varying the salt concentration from 0 to 1M of NaCl, which shows that electrostatic interactions are not the major factor inducing the high unfolding transition temperature. However, the thermodynamic parameters of *Mj*TRX investigated by DSC and CD shows possible clues leading to the high unfolding transition temperature. First although the ΔG_{max} of *Mj*TRX (9.9 Kcal·mol^{-1}) was not much different from that of *E*TRX (9.0 Kcal·mol^{-1}), the corresponding temperature to the ΔG_{max} of unfolding is shifted to about 20 °C higher than that of *E*TRX. Second, the residual ΔH of *Mj*TRX (10.9 cal·g^{-1}) is lower than that of *E*TRX (13.4 cal·g^{-1}) at 116 °C. Third, entropy of the unfolding of *Mj*TRX (3.09 cal residue^{-1}·K^{-1}) is lower than that of *E*TRX (3.97 cal residue^{-1}·K^{-1}) at 116 °C. And fourth, heat capacity of *Mj*TRX (1.41 Kcal·mol^{-1}·K^{-1}) is lower than that of *E*TRX (1.66 Kcal·mol^{-1}·K^{-1}). These results indicate that the thermodynamic stability of *Mj*TRX is not much higher compared to mesophilic protein but the unfolding transition temperature is higher because the temperature of maximum stability is shifted to the higher temperature compared to the mesophilic protein. The maximum free energy is similar to that of *E*TRX because enthalpy and entropy of the unfolding are decreased simultaneously. By definition, Gibb's free energy of the unfolding ($\Delta G = \Delta H - T\Delta S$) would be the same if the degree of reduction in both enthalpy and entropy were the same. In the case of *Mj*TRX, enthalpy of the unfolding is lower than *E*TRX at a given temperature. If we assume that enthalpies of the unfolded state of both *Mj*TRX and *E*TRX are similar, lower enthalpy of the unfolding indicates the higher enthalpy, fewer interactions, in the folded state of protein. So, the fewer interactions and resulting higher flexibility of *Mj*TRX in the folded state is responsible for the low enthalpy and low entropy of the unfolding. Another factor affecting entropy of the

unfolding is the number of proline residues. The numbers of proline per 100 amino acid residues are 7.95 and 4.63 for *Mj*TRX and *E*TRX, respectively. So, the entropy in the unfolded state would be lower in *Mj*TRX than in *E*TRX. Low entropy in the unfolded state due to many prolines and high entropy in the folded state due to the fewer interactions reduce the entropy of the unfolding. The entropy of the unfolding in aqueous media includes two components: one is associated with the increase of configurational freedom in the polypeptide chain and the other with the hydration of groups that become exposed on unfolding. Hydration entropy is proportional to the water accessible surface area, and decreases in magnitude with temperature, vanishing at about 125 °C.[39] Therefore, it is usually assumed that at 120 ~ 130 °C, hydration effects do not contribute to the entropy of protein unfolding in aqueous media, and at this temperature, the measured values correspond to the configurational entropy of unfolding.[40-42] Because the T_m of hyperthermophilic proteins is mostly above 100°C, the value of entropy that affects the stability of hyperthermophilic protein is conformational entropy. Consequently, reduced flexibility of polypeptide backbone and side chain in the unfolded state also contributes to protein stability. In the case of *Mj*TRX, weaker interactions in the folded state and many prolines are likely to be associated with the reduced entropy of unfolding.

Then, why does *Mj*TRX have a higher unfolding transition temperature? We can find the reason from the lower entropy. The maximum stability of protein is obtained at the temperature where the entropy of unfolding becomes zero (Eq. 2).

$$\Delta S = \Delta S_o + \Delta C_p \ln (T / T_o) = 0 \qquad \text{(Eq. 2)}$$

$$T_{max} = \exp (-\Delta S_o / \Delta C_p)^* T_o \qquad \text{(Eq. 3)}$$

(Eq. 3) indicates that the temperature of maximum stability (T_{max}) is dependent on the entropy and heat capacity of unfolding. Low entropy and/or high heat capacity of unfolding shifts the temperature of maximum stability to the higher temperature. However, the high heat capacity increases the steepness of the free energy curve, thereby decreasing the transition temperature of the unfolding.

The transition temperature of the unfolding of the protein becomes higher by, i) increasing the maximum free energy, ii) lowering heat capacity, which flattens the free

energy curve or iii) shifting the temperature of maximum stability to higher temperature. In the case of *Mj*TRX, the transition temperature of the unfolding becomes extremely high by decreasing entropy of the unfolding and simultaneously flattening the free energy curve by lowering the heat capacity. Although the ratio of entropy to heat capacity affects the temperature of maximum stability, the degree of change in entropy was bigger than the heat capacity, resulting in the higher temperature of maximum stability.

Heat capacity of the unfolding is associated with the solvent accessible surface area. While more buried non-polar solvent accessible surface area increases heat capacity, more buried polar solvent accessible surface area decreases heat capacity. After all, less buried non-polar solvent accessible surface area and/or more buried polar solvent accessible surface area would decreases heat capacity. In *Mj*TRX, the changes of a non-polar and polar solvent accessible surface area by unfolding are 70.1±0.8 $Å^2$/residue and 40.4±0.5 $Å^2$/residue, respectively compared to 78.9 $Å^2$/residue and 43.7 $Å^2$/residue for *E*TRX. This analysis indicates that *Mj*TRX has lower heat capacity due to the less buried non-polar solvent accessible area.

In conclusion, *Mj*TRX has high unfolding transition temperature by decreasing entropy of the unfolding, although the maximum free energy of protein is similar to that of the mesophilic protein. The decreased entropy of unfolding is associated with the reduced enthalpy of unfolding and resulting increased flexibility in the folded state and the reduced chain entropy in the unfolded state due to the increased number of prolines. In addition, the buried non-polar solvent accessible area is smaller resulting in lower heat capacity of unfolding, which flattens the free energy curve contributing to a high unfolding transition temperature.

REFERENCES

1. Matsumura, M., Becktel, W. J., Levitt, M. & Matthews, B. W. (1989). Stabilization of phage T4 lysozyme by engineered disulfide bonds. *Proc Natl Acad Sci U S A* **86**(17), 6562-6.
2. Elcock, A. H. (1998). The stability of salt bridges at high temperatures: implications for hyperthermophilic proteins. *J Mol Biol* **284**(2), 489-502.

3. Hennig, M., Darimont, B., Sterner, R., Kirschner, K. & Jansonius, J. N. (1995). 2.0 A structure of indole-3-glycerol phosphate synthase from the hyperthermophile Sulfolobus solfataricus: possible determinants of protein stability [see comments]. *Structure* **3**(12), 1295-306.
4. Jaenicke, R. & Bohm, G. (1998). The stability of proteins in extreme environments. *Curr Opin Struct Biol* **8**(6), 738-48.
5. Korndorfer, I., Steipe, B., Huber, R., Tomschy, A. & Jaenicke, R. (1995). The crystal structure of holo-glyceraldehyde-3-phosphate dehydrogenase from the hyperthermophilic bacterium Thermotoga maritima at 2.5 A resolution. *J Mol Biol* **246**(4), 511-21.
6. Lim, J. H., Yu, Y. G., Han, Y. S., Cho, S., Ahn, B. Y., Kim, S. H. & Cho, Y. (1997). The crystal structure of an Fe-superoxide dismutase from the hyperthermophile Aquifex pyrophilus at 1.9 A resolution: structural basis for thermostability. *J Mol Biol* **270**(2), 259-74.
7. Tanner, J. J., Hecht, R. M. & Krause, K. L. (1996). Determinants of enzyme thermostability observed in the molecular structure of Thermus aquaticus D-glyceraldehyde-3-phosphate dehydrogenase at 25 Angstroms Resolution. *Biochemistry* **35**(8), 2597-609.
8. Watanabe, K., Chishiro, K., Kitamura, K. & Suzuki, Y. (1991). Proline residues responsible for thermostability occur with high frequency in the loop regions of an extremely thermostable oligo-1,6- glucosidase from Bacillus thermoglucosidasius KP1006. *J Biol Chem* **266**(36), 24287-94.
9. Teplyakov, A. V., Kuranova, I. P., Harutyunyan, E. H., Vainshtein, B. K., Frommel, C., Hohne, W. E. & Wilson, K. S. (1990). Crystal structure of thermitase at 1.4 A resolution. *J Mol Biol* **214**(1), 261-79.
10. Dekker, K., Yamagata, H., Sakaguchi, K. & Udaka, S. (1991). Xylose (glucose) isomerase gene from the thermophile Thermus thermophilus: cloning, sequencing, and comparison with other thermostable xylose isomerases. *J Bacteriol* **173**(10), 3078-83.
11. Vieille, C. & Zeikus, G., J. (2001). Hyperthermophilic Enzymes: Sources, Uses, and Molecular Mechanisms for Thermostability. *Microbiol Mol Biol Rev* **65**(1), 1-43.
12. Langsetmo, K., Fuchs, J. A. & Woodward, C. (1991). The conserved, buried aspartic acid in oxidized Escherichia coli thioredoxin has a pKa of 7.5. Its titration produces a

related shift in global stability. *Biochemistry* **30**(30), 7603-9.

13. Wishart, D. S., Boyko, R. F., Willard, L., Richards, F. M. & Sykes, B. D. (1994). SEQSEE: a comprehensive program suite for protein sequence analysis. *Comput Appl Biosci* **10**(2), 121-32.
14. Santoro, M. M. & Bolen, D. W. (1992). A test of the linear extrapolation of unfolding free energy changes over an extended denaturant concentration range. *Biochemistry* **31**(20), 4901-7.
15. Zhang, O., Kay, L. E., Olivier, J. P. & Forman-Kay, J. D. (1994). Backbone 1H and 15N resonance assignments of the N-terminal SH3 domain of drk in folded and unfolded states using en hanced-sensitivity pulsed field gradient NMR techniques. *J Biomol NMR***4**(6), 845-58.
16. Kuboniwa, H., Grzesiek, S., Delaglio, F. & Bax, A. (1994). Measurement of HN-H alpha J couplings in calcium-free calmodulin using new 2D and 3D water-flip-back methods. *J Biomol NMR* **4**(6), 871-8.
17. Grzesiek, S. & Bax, A. (1993). Correlation of backbone amide and aliphatic side-chain resonances in 13C/15N- enriched proteins by isotropic mixing of 13C magnetization. *J Magn Reson B* **101**, 114-119.
18. Ikura, M., Kay, L. E. & Bax, A. (1990). A novel approach for sequential assignment of 1H, 13C, and 15N spectra of proteins: heteronuclear triple-resonance three-dimensional NMR spectroscopy. Application to calmodulin. *Biochemistry* **29**(19), 4659-67.
19. Pascal, S. M., Singer, A. U., Gish, G., Yamazaki, T., Shoelson, S. E., Pawson, T., Kay, L. E. & Forman-Kay, J. D. (1994). Nuclear magnetic resonance structure of an SH2 domain of phospholipase C-gamma 1 complexed with a high affinity binding peptide. *Cell* **77**(3), 461-72.
20. Muhandiram, D. R. & Kay, L. E. (1994). Gradient-enhanced triple-resonance three-dimentional NMR experiments with improved sensitivity. *J Magn Reson B* **103**, 203-216.
21. Delaglio, F., Grzesiek, S., Vuister, G. W., Zhu, G., Pfeifer, J. & Bax, A. (1995). NMRPipe: a multidimensional spectral processing system based on UNIX pipes. *J Biomol NMR* **6**(3), 277-93.
22. Wishart, D. S. & Sykes, B. D. (1994a). The 13C chemical-shift index: a simple method for the identification of protein secondary structure using 13C chemical-shift data. *J*

Biomol NMR **4**(2), 171-80.

23.Clore, G. M., Bax, A. & Gronenborn, A. M. (1991). Stereospecific assignment of beta-methylene protons in larger proteins using 3D 15N-separated Hartmann-Hahn and 13C-separated rotating frame Overhauser spectroscopy. *J Biomol NMR* **1**(1), 13-22.

24. Garrett, D. S., Kuszewski, J., Hancock, T. J., Lodi, P. J., Vuister, G. W., Gronenborn, A. M. & Clore, G. M. (1994). The impact of direct refinement against three-bond HN-C alpha H coupling constants on protein structure determination by NMR. *J Magn Reson B* **104**(1), 99-103.

25. Brunger, A. T. (1993). *X-PLOR manual Version 3.1*, Yale University, New Haven, CT.

26. Wishart, D. S. & Sykes, B. D. (1994b). Chemical Shifts as a Tool for Structure Determination. *Methods Enzymol.* **239**, 363-392.

27. Wuthrich, K. (1986). *NMR of Proteins and Nucleic Acids*, 4, John Wiley and Sons, New York.

28. Kuszewski, J., Gronenborn, A. M. & Clore, G. M. (1996). Improving the quality of NMR and crystallographic protein structures by means of a conformational database potential derived from structure databases. *Protein Sci* **5**(6), 1067-80.

29. Kuszewski, J., Gronenborn, A. M. & Clore, G. M. (1997). Improvements and extensions in the conformational database potential for the refinement of NMR and X-ray structures of proteins and nucleic acids. *J Magn Reson* **125**(1), 171-7.

30. McCray, B. S., Edmondson, S. P. & Shriver, J. W. (1996). Hyperthermophile protein folding thermodynamics: Differential scanning calorimetry and chemical denaturation of Sac7d. *J. Mol. Biol.* **264**, 784-805.

31. Pfeil, W., Gesierich, U., Kleemann, G. R. & Sterner, R. (1997). Ferredoxin from the hyperthermophile Thermotoga maritima is stable beyond the boiling point of water. *J. Mol. Biol.* **272**, 591-596.

32. Privalov, P. L. & Potekhin, S. A. (1986). Scanning microcalorimetry in studying temperature-induced changes in proteins. *Methods Enzymol* **131**, 4-51.

33. Richardson, J. M., 3rd, Lemaire, S. D., Jacquot, J. P. & Makhatadze, G. I. (2000). Difference in the mechanisms of the cold and heat induced unfolding of thioredoxin h from Chlamydomonas reinhardtii: spectroscopic and calorimetric studies. *Biochemistry* **39**(36), 11154-62.

34. Rees, D. C. & Robertson, A. D. (2001). Some thermodynamic implications for the thermostability of proteins. *Protein Sci* **10**(6), 1187-94.

35. Lee, D. Y., Ahn, B. Y. & Kim, K. S. (2000). A thioredoxin from the hyperthermophilic archaeon Methanococcus jannaschii has a glutaredoxin-like fold but thioredoxin-like activities. *Biochemistry* **39**(22), 6652-9.

36.Cave, J. W., Cho, H. S., Batchelder, A. M., Yokota, H., Kim, R. & Wemmer, D. E. (2001) Solution nuclear magnetic resonance structure of a protein disulfide oxidoreductase from Methanococcus jannaschii. *Protein Sci* **10**(2), 384-96.

37. Yip, K. S., Stillman, T. J., Britton, K. L., Artymiuk, P. J., Baker, P. J., Sedelnikova, S. E., Engel, P. C., Pasquo, A., Chiaraluce, R. & Consalvi, V. (1995). The structure of Pyrococcus furiosus glutamate dehydrogenase reveals a key role for ion-pair networks in maintaining enzyme stability at extreme temperatures [see comments]. *Structure* **3**(11), 1147-58.

38. Ogasahara, K., Lapshina, E. A., Sakai, M., Izu, Y., Tsunasawa, S., Kato, I. & Yutani, K. (1998). Electrostatic stabilization in methionine aminopeptidase from hyperthermophile Pyrococcus furiosus. *Biochemistry* **37**(17), 5939-46.

39. Makhatadze, G. I. & Privalov, P. L. (1996). On the entropy of protein folding. *Protein Sci* **5**(3), 507-10.

40. Lee, K. H., Xie, D., Freire, E. & Amzel, L. M. (1994). Estimation of changes in side chain configurational entropy in binding and folding: general methods and application to helix formation. *Proteins* **20**(1), 68-84.

41. Murphy, K. P., Freire, E. & Paterson, Y. (1995). Configurational effects in antibody-antigen interactions studied by microcalorimetry. *Proteins* **21**(2), 83-90.

42. Murphy, K. P., Xie, D., Garcia, K. C., Amzel, L. M. & Freire, E. (1993). Structural energetics of peptide recognition: angiotensin II/antibody binding. *Proteins* **15**(2), 113-20.

43. Laskowski, R. A., Rullmannn, J. A., MacArthur, M. W., Kaptein, R. & Thornton, J. M. (1996). AQUA and PROCHECK-NMR: programs for checking the quality of protein structures solved by NMR. *J Biomol NMR* **8**, 477-86.

44. Kraulis, P. J. (1991). MOLSCRIPT: A Program to Produce Both Detailed and Schematic Plots of Protein Structures. *Journal of Applied Crystallography* **24**, 946-950.

45. Merritt, Ethan, A., Bacon & David, J. (1997). Raster3D - photorealistic molecular

graphics. *Methods Enzymol* **277**, 505-524.

46. Nicholls, A., Sharp, K. A. & Honig, B. (1991). Protein folding and association: insights from the interfacial and thermodynamic properties of hydrocarbons. *Proteins* **11**(4), 281-96.